SCENE CHANGE ARTIFACTS IN FOURIER TRANSFORM SPECTROSCOPY OF TEMPORALLY CHANGING SOURCES

THESIS

Anthony M. Young, Second Lieutenant, USAF

AFIT/GAP/ENP/10-M16

DEPARTMENT OF THE AIR FORCE
AIR UNIVERSITY

AIR FORCE INSTITUTE OF TECHNOLOGY

Wright-Patterson Air Force Base, Ohio

The views expressed in this thesis are those of the author and do not reflect the official policy or position of the United States Air Force, Department of Defense, or the U.S. Government.

AFIT/GAP/ENP/10-M16

SCENE CHANGE ARTIFACTS IN FOURIER TRANSFORM SPECTROSCOPY OF TEMPORALLY CHANGING SOURCES

THESIS

Presented to the Faculty

Department of Engineering Physics

Graduate School of Engineering and Management

Air Force Institute of Technology

Air University

Air Education and Training Command

In Partial Fulfillment of the Requirements for the

Degree of Master of Science in Applied Physics

Anthony M. Young, BS

Second Lieutenant, USAF

March 2010

AFIT/GAP/ENP/10-M16

SCENE CHANGE ARTIFACTS IN FOURIER TRANSFORM SPECTROSCOPY OF TEMPORALLY CHANGING SOURCES

Anthony M. Young, BS

Second Lieutenant, USAF

Approved:

_____	_____
Dr. Kevin Gross (Chairman)	Date
_____	_____
Dr. Glen Perram (Member)	Date
_____	_____
Dr. Christoph Borel (Member)	Date

Abstract

Improved understanding of midwave infrared (1-5 micron) spectral emissions from detonation fireballs is needed to develop phenomenological models for battle space optical forensics. The ability to measure radiance over a wide band pass at arbitrary resolutions make Fourier-transform spectrometers (FTS) an attractive tool. However, interferometer based spectroscopic measurements can be corrupted when the observed intensity changes during data acquisition. While small, random fluctuations in scene intensity translate into noise, systematic variations introduce scene-change artifacts (SCAs) into Fourier-transformed spectrum. Approximating a detonation fireball as a blackbody radiator, modified with an atmospheric attenuation τ_{atm}, with an exponentially cooling temperature $T(t) = T_0 e^{-kt}$, double sided interferograms from an ideal Michelson interferometer were simulated and converted to a measured spectrum L_m to characterize the nature and magnitude of SCAs. With $T_0 = 1500K$, changing scene spectra on $0 < \tilde{\nu} < 7900cm^{-1}$ at $\delta\tilde{\nu} = 0.04cm^{-1}$ resolution were computed with percent changes in $T(t)$ between 0 and 80%. The real part of L_m ($\mathrm{Re}\{L_m\}$) is well approximated by the instantaneous spectrum (L_{ZPD}) at zero path difference. Differences between $\mathrm{Re}\{L_m\}$ and L_{ZPD} ($\mathrm{Re}\{L_m\} - L_{ZPD}$) is largest when τ_{atm} is highly structured and these differences increase with the amount of temperature change during the measurement. Similarly, the imaginary part of L_m ($\mathrm{Im}\{L_m\}$) exhibits highly structured features whenever τ_{atm}

changes rapidly with ν. In general, $\mathrm{Im}\{L_m\} > \mathrm{Re}\{L_m\} - L_{ZPD}$ agreeing with previous theoretical work and the increase in magnitude of $\mathrm{Im}\{L_m\}$ with temperature change is more pronounced than $\mathrm{Re}\{L_m\} - L_{ZPD}$. These trends were independent of initial temperature, spectral resolution, or choice of τ_{atm}. For a MOPD = .5cm, a 4% reduction in temperature during a single scan produced an RMS value of $5\mu W / sr / cm^2 / cm^{-1}$ in $\mathrm{Im}\{L_m\}$. A 27% temperature change was needed to produce the same RMS value for $\mathrm{Re}\{L_m\} - L_{ZPD}$. For comparison, the RMS value of L_{ZPD} was $507\mu W / sr / cm^2 / cm^{-1}$ and $125\mu W / sr / cm^2 / cm^{-1}$ for a 20% and 60% temperature change, respectively.

SCAs were also studied with an ABB/Bomem MR-154 FTS by measuring a time-varying broadband source. Using an Oriel Q-series incandescent lamp, the FTS operating at $1cm^{-1}$ resolution observed the changing spectral radiance as the lamp's input power was smoothly varied during interferogram acquisition. A 2.52% relative change in ZPD voltage during the scan produced a few spectral lines in $\mathrm{Im}\{L_m\}$ that were 54.8% above the instrument RMS NESR.

Acknowledgments

I would like to express my sincere appreciation to my faculty advisor, Dr. Kevin Gross, for his guidance and support throughout the course of this thesis effort. The insight and experience was certainly appreciated. A special thanks to Dr. Glen Perram and Dr. Christoph Borel for being a part of my committee and the laboratory technicians Greg Smith and Mike Ranft for the help in acquiring and setting up equipment.

Anthony M. Young

This Note is not to be included with the Acknowledgments – it is for information only: ***It is prohibited to include any personal information in the following categories about U.S. citizens, DOD Employees and military personnel: social security account numbers; home addresses; dates of birth; telephone numbers other than duty officers which are appropriately made available to the general public; names, locations and any other identifying information about family members of DOD employees and military personnel.***

Table of Contents

Page

List of Figures

Figure Page

Figure Page

SCENE CHANGE ARTIFACTS IN FOURIER TRANSFORM SPECTROSCOPY OF TEMPORALLY CHANGING SOURCES

I. Introduction

Background

Numerous defense and civilian applications require spectral measurement of temporally evolving sources. Civilian applications may remove scene change effects through repeated sampling which, at its simplest, amounts to averaging out the errors. Many defense applications can ill afford the luxury of repeated sampling. The events are either singular as is the case with muzzle flashes and Improvised Explosive Devices (IEDs), or reaction is time critical as is the case with rocket plumes. Using interpreted spectra to determine the nature of an explosive device is a critical tool in battlespace awareness and forensics.

The Air Force Institute of Technology Remote Sensing Group (AFIT RSG) is pursuing measurements of transient events to develop phenomenological models for battlespace events. One tool in use to acquire these signatures is Fourier transform spectroscopy (FTS) which allows the investigation of spectrally interesting phenomena. The chemicals in explosions produce similar spectra, but over small frequency bands, unique features create the possibility to investigate compositions and concentrations to better classify chemical reagents. Most of the bands of interest are molecular bands in the infrared where FTS is strongly suited for analysis. FTS provides many benefits over other spectral instruments such as radiometers and grating spectrometers. When viewing transient events, the number of photons reaching observation equipment can be small,

especially when viewing at great distances, also making FTS more suitable than a grating spectrometer. FTS is able to view large frequency ranges at high resolution where a grating spectrometer might require multiple gratings to view all the bands of interest.

For many systems, chemical concentrations and temperatures can be revealed through FTS techniques. During many transient events of interest, the scene changes over a time interval of data acquisition causing changes in interferogram intensity not caused by an optical path length difference. The nature of quickly changing scenes on FTS calculated spectra is not well understood and needs to be characterized for correct scene interpretation to exploit transient event signatures. Using FTS to acquire transient event signatures might seem counterintuitive because of their rapid nature; however, previous observations from AFIT RSG of transient events have captured meaningful spectra[1]. The extent to which the spectra are corrupted needs to be investigated to determine when certain approximations and certain conditions can provide accurate FTS spectra even when the scene is changing rapidly.

Objectives

This research intends to describe the effect of exponential temperature decays in black body radiance profiles on spectra produced through an ideal FTS system and to determine the validity of using the zero path difference (ZPD) spectrum, the instantaneous spectrum corresponding to when the Michelson is at ZPD, as an approximation of the calculated real spectrum for an exponentially cooling black body. Also whether the calculated real spectrum corruption can be inferred based upon the imaginary spectrum and how it relates to the calculated real spectrum as a function of

temperature change. This will help determine the conditions when FTS is corrupted through scene change and when it is viable for observing such transient events. This work primarily looks at RMS values to quantitatively look at entire spectra. A more in depth look of specific spectral features would also be beneficial for analysis of spectral features used in forensic analysis.

II. Theory

FTS background and introduction to the complex spectrum

A Michelson interferometer splits incident light into two paths. Within one arm of the interferometer, the path length is changed and when the light is recombined, interference occurs. The intensity of the recombined light is measured as a function of optical path difference (OPD) and the intensity of the interferogram given by Brault will follow[2]

$$I_m(x) = \int_0^\infty \eta(\tilde{\nu})\eta_m(\tilde{\nu})^{-1}L(\tilde{\nu})d\tilde{\nu} + \int_0^\infty \eta(\tilde{\nu})L(\tilde{\nu})\cos(2\pi x\tilde{\nu})d\tilde{\nu}\,, \tag{1}$$

where

$$\int_0^\infty \eta(\tilde{\nu})\eta_m(\tilde{\nu})^{-1}L(\tilde{\nu})d\tilde{\nu} \tag{2}$$

is the DC component of the interferogram and

$$\int_0^\infty \eta(\tilde{\nu})L(\tilde{\nu})\cos(2\pi x\tilde{\nu})d\tilde{\nu} \tag{3}$$

is the AC component.

$\eta(\tilde{\nu})$ is the interferometer efficiency and is given by the expression

$$\frac{1}{2}\eta_b(\tilde{\nu})\eta_o(\tilde{\nu})\,. \tag{4}$$

$\eta_b(\tilde{\nu})$ is the beam splitter efficiency and is given by the expression

$$\eta_b(\tilde{\nu}) = 4R(\tilde{\nu})T(\tilde{\nu}) \tag{5}$$

where $R(\tilde{\nu})$ is the wavenumber dependent reflectance of the beam splitter and $T(\tilde{\nu})$ is the wavenumber dependent transmittance of the beam splitter. For an ideal case, half of the

incident light at every wavenumber is reflected and half is transmitted resulting in $\eta_b(\tilde{\nu}) = \frac{1}{2}$. $\eta_o(\tilde{\nu})$ is the efficiency of all the other optics and would be unity in the ideal case. $\eta_m(\tilde{\nu})$ is the modulator efficiency which is the ZPD amplitude divided by the averaged baseline modulation amplitude of the interferogram. The ideal case also ignores the wavenumber dependent phase shift, $\phi_{\tilde{\nu}}$, caused by all optics in the interferometer. The AC component of the interferogram can be expressed as

$$I(x) = \int_0^\infty \eta(\tilde{\nu}) L(\tilde{\nu}) \cos(2\pi\tilde{\nu}x - \phi_{\tilde{\nu}}) d\tilde{\nu} \,. \tag{6}$$

The remaining components creating the interferogram are $L(\tilde{\nu})$, the incident spectral radiance, and x, the OPD. Only the AC component is needed at this point to continue.

From simplifications found in Sromovsky,[3] a complex spectrum $G(\tilde{\nu})$ defined for all $\tilde{\nu}$ can be introduced as

$$G(\tilde{\nu}) = \begin{cases} \frac{1}{2}\eta(\tilde{\nu}) L(\tilde{\nu}) \exp(i\phi_{\tilde{\nu}}), \tilde{\nu} > 0 \\ \frac{1}{2}\eta(-\tilde{\nu}) L(-\tilde{\nu}) \exp(-i\phi_{-\tilde{\nu}}), \tilde{\nu} < 0 \end{cases} . \tag{7}$$

The real transform of the complex spectrum will yield the interferogram shown by

$$I(x) = \int_{-\infty}^\infty G(\tilde{\nu}) \exp(-2\pi i\tilde{\nu}x) d\tilde{\nu} \,. \tag{8}$$

Consequently, the spectrum is now given by the complex Fourier transform of the real interferogram[4]. The original spectrum can now be defined in terms of this transform as

$$L(\tilde{\nu}) = \frac{2}{\eta(\tilde{\nu})} \exp(-i\phi_{\tilde{\nu}}) \int_{-\infty}^\infty I(x) \exp(2\pi i x\tilde{\nu}) dx \,. \tag{9}$$

For a typical Michelson interferometer which produces interferograms that are discretely sampled at uniform OPDs, a discrete Fourier transform best represents the spectrum. The limits of integration with respect to OPD are finite and the Fourier transform defining the spectrum is best approximated through the finite series

$$H(\tilde{\nu}) \approx \frac{2X}{N} \sum_{k=-N/2}^{N/2-1} I(x_k) \exp(2\pi i \tilde{\nu} x_k) \tag{10}$$

where X is maximum OPD (MOPD) and N is the number of points in the interferogram. If $|\tilde{\nu}| < \frac{N}{4X}$, then the spectrum is sampled adequately and can be represented by only N wavenumbers given by [5]

$$H(\tilde{\nu}_n) = \frac{2X}{N} \sum_{k=-N/2}^{N/2-1} I(x_k) \exp(2\pi i n k / N) \tag{11}$$

where

$$\tilde{\nu}_n = \frac{n}{2X} \tag{12}$$

and

$$n = -N/2, -N/2+1, ..., N/2-1. \tag{13}$$

The preceding development assumes a static source, $L(\tilde{\nu})$; one that is constant during the measurement. If the radiance of the incident light changes while the device is scanning, scene change artifacts (SCAs) in the spectrum result from changes in interferogram not caused by a change in optical path length difference.

Previous theoretical scene change work

The nature of SCAs can be better understood by considering smooth time varying sources. Following previous work from Kick et al.[6] and using an ideal Michelson interferometer so there are no phase errors, if a scene were changing linearly with time, shown in Figure 1, the spectrum could be given by

$$L(t,\tilde{\nu}) = L_1(\tilde{\nu}) + \frac{t}{t_{tot}}\left(L_3(\tilde{\nu}) - L_1(\tilde{\nu})\right) \tag{14}$$

where t_{tot} is the total measurement time, $L_1(\tilde{\nu})$ is the spectral radiance at the beginning of the measurement, and $L_3(\tilde{\nu})$ is the spectral radiance at the end of the measurement. As time passes, the radiance at each wavenumber changes linearly from $L_1(\tilde{\nu})$ to $L_3(\tilde{\nu})$ until $t = t_{tot}$.

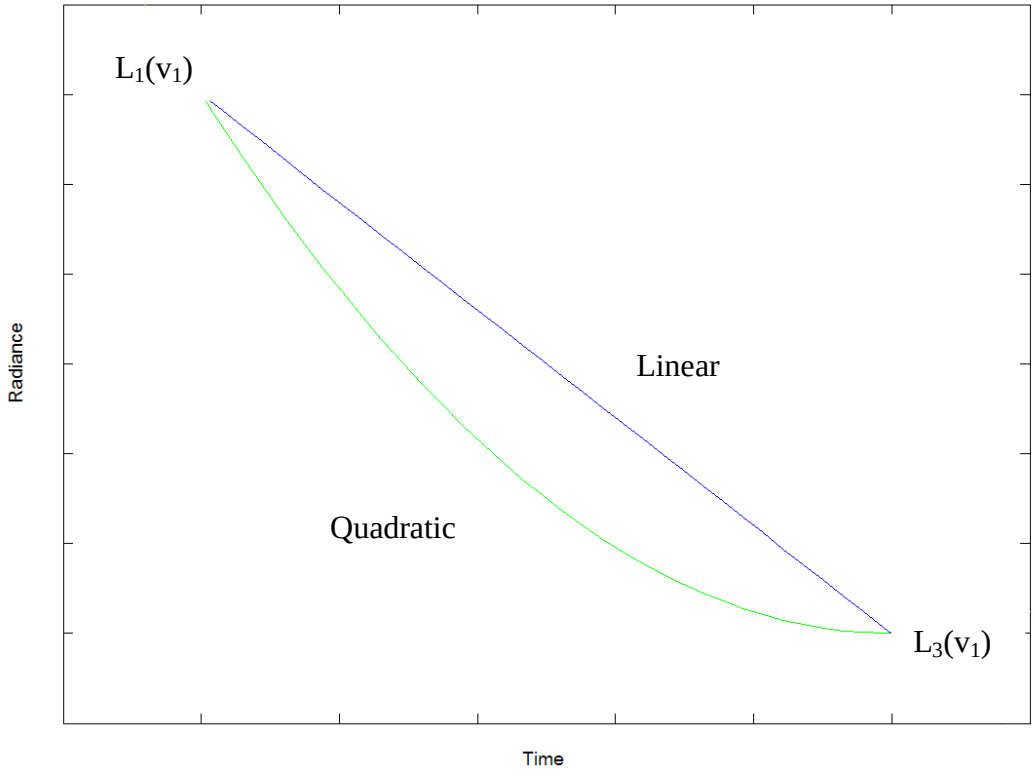

Figure 1. Linear (blue) and quadratic (green) variations in radiance with time for a single wavenumber.

With a change in variables from time to path difference, the spectral radiance as a function of wavenumber and path difference is given by

$$L(x,\tilde{\nu}) = \frac{L_1(\tilde{\nu}) + L_3(\tilde{\nu})}{2} + \frac{x}{\Delta x}(L_3(\tilde{\nu}) - L_1(\tilde{\nu})) \tag{15}$$

where Δx is the total distance the mirror scans and x is the instantaneous path difference and ranges from $-\frac{\Delta x}{2}$ to $\frac{\Delta x}{2}$. The interferogram from a continually sampling spectrometer would then be the inverse Fourier transform of Equation (15) given as

$$I(x) = \Im^{-1}\{L(x,\tilde{\nu})\} = \frac{I_1(x) + I_3(x)}{2} + \frac{x}{\Delta x}\left(I_3(x) - I_1(x)\right). \tag{16}$$

This is the interferogram captured by the Michelson. To calculate the spectrum the Fourier transform of the interferogram is needed. Kick et al. show that if Equation (16) is transformed back into a wavenumber domain, the resulting effect on the spectrum is shown by[7]

$$L_m(\tilde{\nu}) = \frac{L_1(\tilde{\nu}) + L_3(\tilde{\nu})}{2} + \frac{i}{2\pi\Delta x}\frac{\partial(L_3(\tilde{\nu}) - L_1(\tilde{\nu}))}{\partial\tilde{\nu}}. \tag{17}$$

The imaginary part comes from the Fourier transform

$$\Im\left\{\frac{x}{\Delta x}\left(I_3(x) - I_1(x)\right)\right\} \tag{18}$$

which uses the Fourier transform relationship

$$\Im\left\{x^n f\left(x\right)\right\} = \left(\frac{i}{2\pi}\right)^n \frac{\partial^n \hat{f}(\nu)}{d\nu^n}. \tag{19}$$

Knowing a linear scene change provides an imaginary theoretical component

$$Yi = \mathrm{Im}(L_m(\tilde{\nu})) = \frac{i}{2\pi\Delta x}\frac{\partial(L_3(\tilde{\nu}) - L_1(\tilde{\nu}))}{\partial\tilde{\nu}}, \tag{20}$$

the imaginary part of the spectrum can be used to distinguished SCAs.

Similarly, the same analysis can be used for a scene radiance that is changing quadratically with time, shown in Figure 1, resulting in

$$L_m(\tilde{\nu}) = L_{ZPD}(\tilde{\nu}) - \frac{1}{4\pi^2\Delta x^2}\frac{\partial(2L_1(\tilde{\nu}) - 4L_{ZPD}(\tilde{\nu}) + 2L_3(\tilde{\nu}))}{\partial\tilde{\nu}^2} + \frac{i}{2\pi\Delta x}\frac{\partial(L_3(\tilde{\nu}) - L_1(\tilde{\nu}))}{\partial\tilde{\nu}} \tag{21}$$

where L_{ZPD} corresponds to the ZPD spectrum observed by the spectrometer[6]. There now is a second order correction to the observed real spectrum given by

$$Yr = -\frac{1}{4\pi^2\Delta x^2}\frac{\partial(2L_1(\tilde{\nu}) - 4L_{ZPD}(\tilde{\nu}) + 2L_3(\tilde{\nu}))}{\partial\tilde{\nu}^2} \tag{22}$$

and the first order correction to the imaginary piece remains the same as the linear case. The same analysis can be used with higher order terms for more accurate approximations.

Connection between previous work and discrete FFT

This analysis is not obviously applicable to the discrete Fourier transform described above and therefore a real Michelson system. In the discrete transform, the OPD does not range from $-\infty$ to ∞, which is necessary for the full transform found in Kick et al. To limit the extent of the integral and to apply their analysis to discrete transforms, let the interferogram intensity equal the convolution given by

$$\tilde{\mathrm{I}}(x) = \mathrm{I}(x) * rect(x, MOPD). \tag{23}$$

This will result in the Fourier transform giving the spectrum as

$$\Im\left\{\tilde{\mathrm{I}}(x)\right\} = \int_{-\infty}^{\infty} e^{i2\pi x\tilde{\nu}}\,\tilde{\mathrm{I}}(x)dx \tag{24}.$$

However, $\tilde{\mathrm{I}}_{\mathrm{m}}(x) = 0$ when $|x| > MOPD$ resulting in

$$\Im\left\{\tilde{\mathrm{I}}(x)\right\} = \int_{-MOPD}^{MOPD} e^{i2\pi x\tilde{\nu}}\,\mathrm{I}(x)dx\,.^{[8]} \tag{25}$$

The spectrum is not continuously sampled, therefore the spectrum given by Equation (25) is discretized and results in Equation (10). This allows for the discrete sampling and finite MOPD characteristics of a Michelson to be represented.

Connection to detonation fireball

Within the realm for detonation fireballs, exponentially decaying models can accurately describe the radiance change over time. Defining a decay constant that controls what

temperature change occurs creating a smoothly varying source over a half scan period for a Michelson allows for comparisons to Kick et al. analysis. When the temperature difference is small enough so the exponential decay creates a spectrum that can accurately be described as a linear or quadratic decay, the real and imaginary spectrum can accurately be described by the mathematics presented in Kick et al. Regardless of the mathematical representation of SCAs, the magnitude of these features can be compared to a noise equivalent spectral radiance, NESR, to see if scene change creates artifacts that rise above the instrument noise floor. This will determine the corruptness of using FTS and if no SCAs are above the inherent noise floor of the system, there is no corruption from SCAs.

III. Modeling

Model introduction

An ideal detonation fireball is modeled as a black body radiator with an exponentially decaying temperature given by

$$B(\tilde{\nu},T(t)) = 2hc^2\tilde{\nu}^3 \frac{1}{e^{\frac{hc\tilde{\nu}}{k_b T(t)}} - 1} \tag{26}$$

where temperature follows

$$T(t) = T_0 e^{-kt} \tag{27}$$

and T_0 is the initial temperature and k is a decay constant. Including atmospheric transmission, $\tau_{atm}(\tilde{\nu})$, resulted in a time-evolving expression for radiance as

$$L(t,\tilde{\nu}) = \tau_{atm}(\tilde{\nu})B(\tilde{\nu},T(t)). \tag{28}$$

By inputting a range of optical path length differences based on a HeNe wavelength sampling, 632.816 nm, an interferogram was created by using the cosine transform

$$y(x_i) = \int_0^\infty D(\tilde{\nu})\eta(\tilde{\nu})L(t_i,\tilde{\nu})\cos(2\pi i x_i\tilde{\nu} - \phi_{\tilde{\nu}})d\tilde{\nu} \tag{29}$$

where $D(\tilde{\nu})$ is the detector response at a given wavenumber and for the model is unity over the wavenumbers from 1800 cm^{-1} to 7900 cm^{-1} and zero elsewhere. $\phi_{\tilde{\nu}}$ is the wavenumber dependent phase shift and in the model was the ideal case of zero. x_i is the optical path length difference of the two interferometer arms corresponding to the i^{th} time interval. $\tilde{\nu}$ is the wavenumbers over which the model is made, and $L(t_i,\tilde{\nu})$ is the spectrum created above at a specific time matching the measurement being made while

$OPD = x_i$. At each successive HeNe wavelength, the spectrum has evolved one time step, so unique values of $L(t_i, \tilde{\nu})$ corresponds to each OPD value, x_i, through the relation

$$x_i = vt_i \tag{30}$$

where v is the mirror velocity.

The model was created over the wavenumber range from 0 cm^{-1} to 7901 cm^{-1}, the Nyquist frequency corresponding to the HeNe wavelength sampling. By allowing the temperature to decay to 20 percent of its initial temperature, the decay constant k could be solved for by knowing the number of points in the interferogram which is equal to the total number of time steps taken.

The number of samples of the frequency axis for a given MOPD must insure the condition $|\tilde{\nu}| < \frac{N}{4X}$ is satisfied. If the frequency axis is not adequately sampled, artifacts not caused by scene change can contribute to the spectrum. Solving for the needed spacing in the frequency axis gives the relationship for the number of points as

$$N_{pts} = Nyquist(2MOPD) \tag{31}$$

but more points are needed to define the derivatives at each spectral coordinate, so using 25 times the output of Equation (31) was more than sufficient to accurately create the derivatives needed to mathematically represent scene change in Equation (21).

The interferogram created through this model will look like Figure 2 and depending on how much the black body is changing in temperature, the baseline modulation amplitude at the beginning, on the left, will be greater than that of the end, on the right, because the intensity of the spectrum is greater at that time.

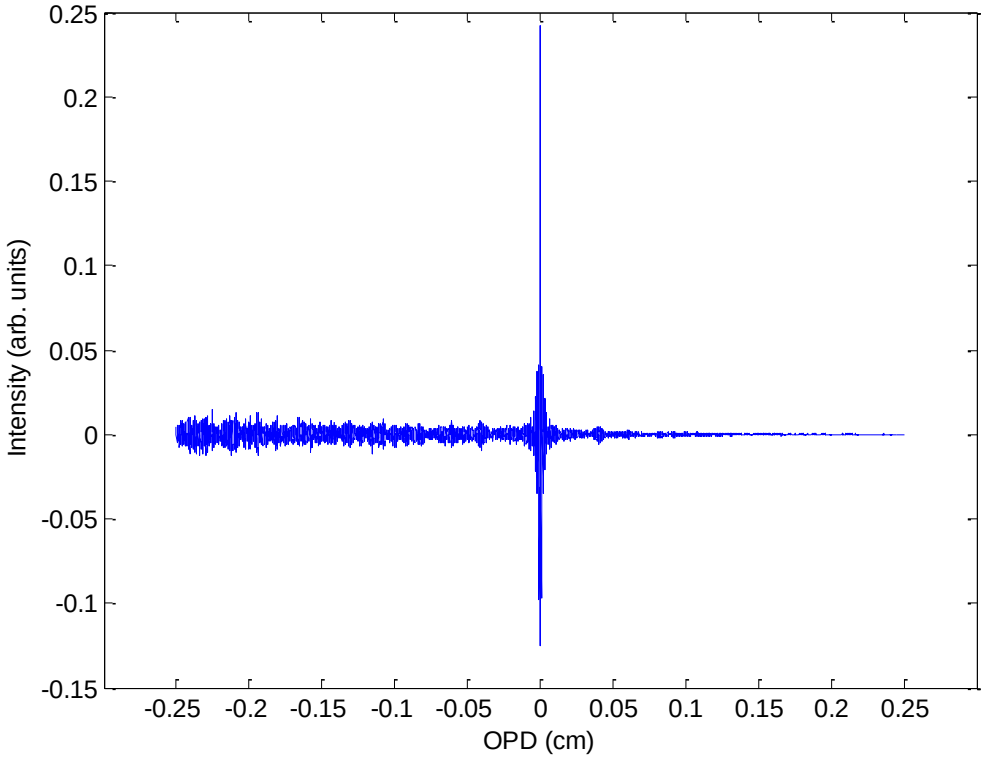

Figure 2. Interferogram of a black body cooling during data acquisition. MOPD= .25 cm. Initial Temperature = 1500 K. Final Temperature = 600 K.

While there is a DC component for the transform because the spectrum is evolving, the AC coupling of the Michelson system is such that the DC component is subtracted faster than the modulated part of the interferogram resulting in an interferogram with a baseline of zero.

The interferogram is transformed through a discrete Fourier transform, given by Equation (11), to give the resulting spectrum and the real and imaginary components are compared to the pieces found in the Kick et al. analysis. The spectrum corresponding to the interferogram in Figure 2 is presented in Figure 3. The spectral features are the

atmospheric transmission features over the given wavenumber region for an atmospheric path length of 0.5 km. The process of turning the interferogram into a spectrum also cancels any effects given by the previous processes. From Equation (9), a factor of a half from the system efficiency factor, $\eta(\tilde{\nu})$, and another factor of two from the conservation of energy in defining a symmetric spectrum defined over all $\tilde{\nu}$ in Equation (7) results in a factor of four being applied to the integral defining the spectrum after the Fourier transform to undo the effects of the interferometer.

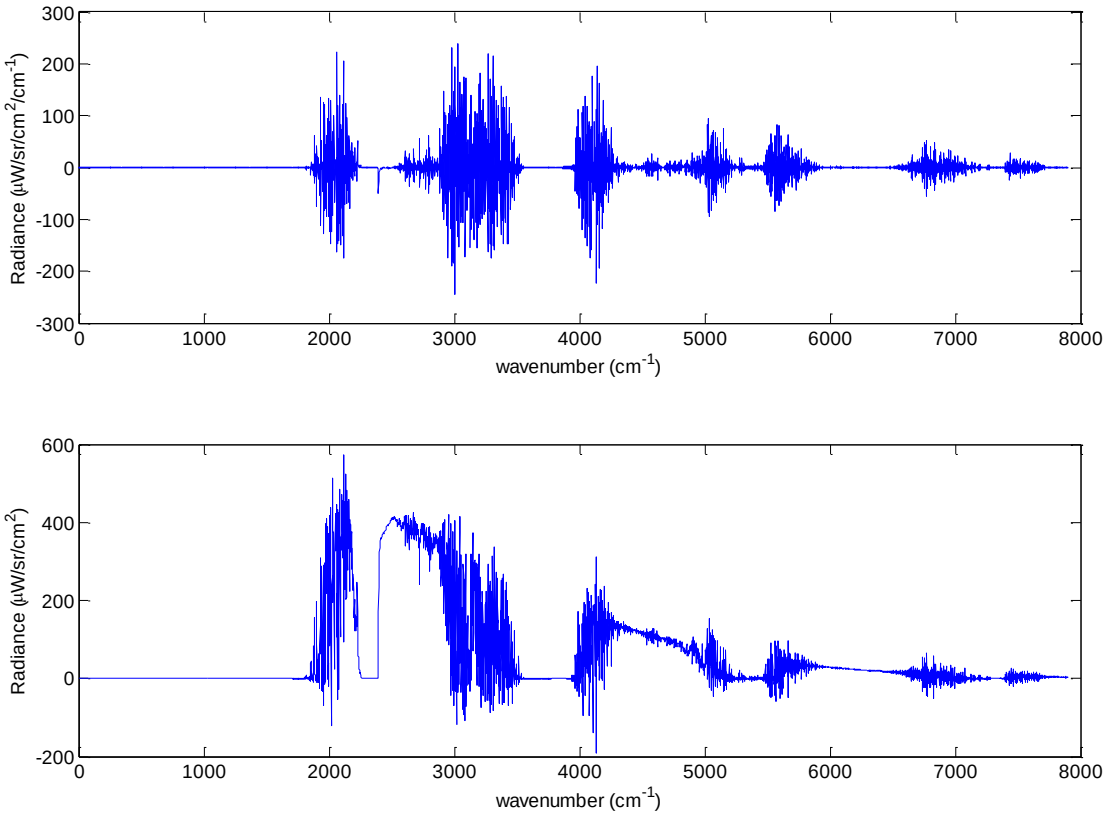

Figure 3. Calculated spectrum from interferogram presented in Figure 2. Imaginary spectrum is on top and real spectrum is on bottom.

The imaginary structures correspond to the regions in the real spectrum where there are abundant spectral features relating to a highly structured τ_{atm}.

Using this model will allow the simulation of a Michelson observing an exponentially cooling black body through atmosphere over 0 to 7901 cm^{-1}. The calculated spectrum can be compared to the Kick et al. analysis. By separating the real and imaginary components and calculating the theoretical components through the derivative found in Equation (21), the implementation of Kick et al. can be verified.

It was unknown as to whether the mathematical treatment in Kick et al. accurately accounts for the spectral information contained in the time evolving nature of scene change. After taking a Fourier transform, this would create spectral information not attributed to the beginning spectrum. To address the problem of aliasing, oversampling was used. With a wavelength as small as 126.4 nm, $\frac{HeNe}{5}$, no spectral features were observed outside of the black body curve up to the Nyquist frequency and no noticeable changes to the spectrum occurred indicating additional spectral information was not present.

Metrics

By modeling a rapidly cooling Planckian, the nature of SCAs can now be examined. Specifically, the measured spectrum $L_m(\tilde{\nu})$ will be compared to L_{ZPD} the instantaneous spectrum at ZPD. For several comparisons, root-mean squared, RMS, values were used to compare trends and entire spectra.

SCA metrics need to be created to help understand the extent to which spectral measurements of evolving sources become corrupted when using FTS. Moreover, being able to determine if scene change is significantly corrupting the real spectrum, $\mathrm{Re}\{L_{\mathrm{m}}\}$, by examining the imaginary spectrum, $\mathrm{Im}\{L_m\}$,would be very beneficial. A useful relationship is comparing the imaginary spectrum to the corruption in the real spectrum given by the difference between $\mathrm{Re}\{L_{\mathrm{m}}\}$ and L_{ZPD}, $\mathrm{Re}\{L_m\} - L_{ZPD}$. Showing the change in the RMS value of $\mathrm{Im}\{L_m\}$ along with the RMS value of $\mathrm{Re}\{L_m\} - L_{ZPD}$ as both evolve as a function of temperature change shows how the connection between increased imaginary components and the deviation from the L_{ZPD}. More specifically, the real SCA RMS magnitude given by

$$SCA_{\mathrm{Re}} = RMS(\mathrm{Re}\{L_m\} - L_{ZPD}) / RMS(\mathrm{Re}\{L_m\}) \tag{32}$$

and the imaginary SCA RMS magnitude

$$SCA_{\mathrm{Im}} = RMS(\mathrm{Im}\{L_m\}) / RMS(\mathrm{Re}\{L_m\}) \tag{33}$$

are used to describe the magnitude of SCAs as they change with certain parameters. Similarly, the maximum real SCA magnitude

$$MSCA_{\mathrm{Re}} = Max(\mathrm{Re}\{L_m\} - L_{ZPD}) / RMS(\mathrm{Re}\{L_m\}) \tag{34}$$

and the maximum imaginary SCA magnitude

$$MSCA_{\mathrm{Im}} = Max(\mathrm{Im}\{L_m\}) / RMS(\mathrm{Re}\{L_m\}) \tag{35}$$

are used for analysis.

For different decay rates, the exponential curve creates a change in the spectrum that can be approximated by a first or second degree polynomial. How well this approximation fits the actual spectrum is seen in the deviation of $\mathrm{Re}\{L_{\mathrm{m}}\}$ from L_{ZPD}. Comparing the difference between the theoretical predictions based on Kick et al. and the actual calculated real spectrum using an exponentially cooling blackbody will ultimately show how well and for what conditions the theoretical predictions are a good mathematical approximation. The trends of the model will be spectrum dependent, however, by comparing different temperature changes and different atmospheric transmission features, a family of curves can be seen with the same general trend. It is also important to consider the magnitude of SCAs and how they compare to a detection instrument's noise equivalent spectral radiance, NESR.

Model analysis

For Figure 4, the exponential temperature decay from 1500 K to 1200 K creates a change in the spectrum that can be closely approximated by a quadratic polynomial at every wavenumber resulting in nearly all lines to be indistinguishable. This allows for the mathematical representation found in Equation (21) to accurately represent scene change. $\mathrm{Re}\{L_m\}$ closely resembles L_{ZPD} with the difference being the second order correction found in the quadratic case, Yr.

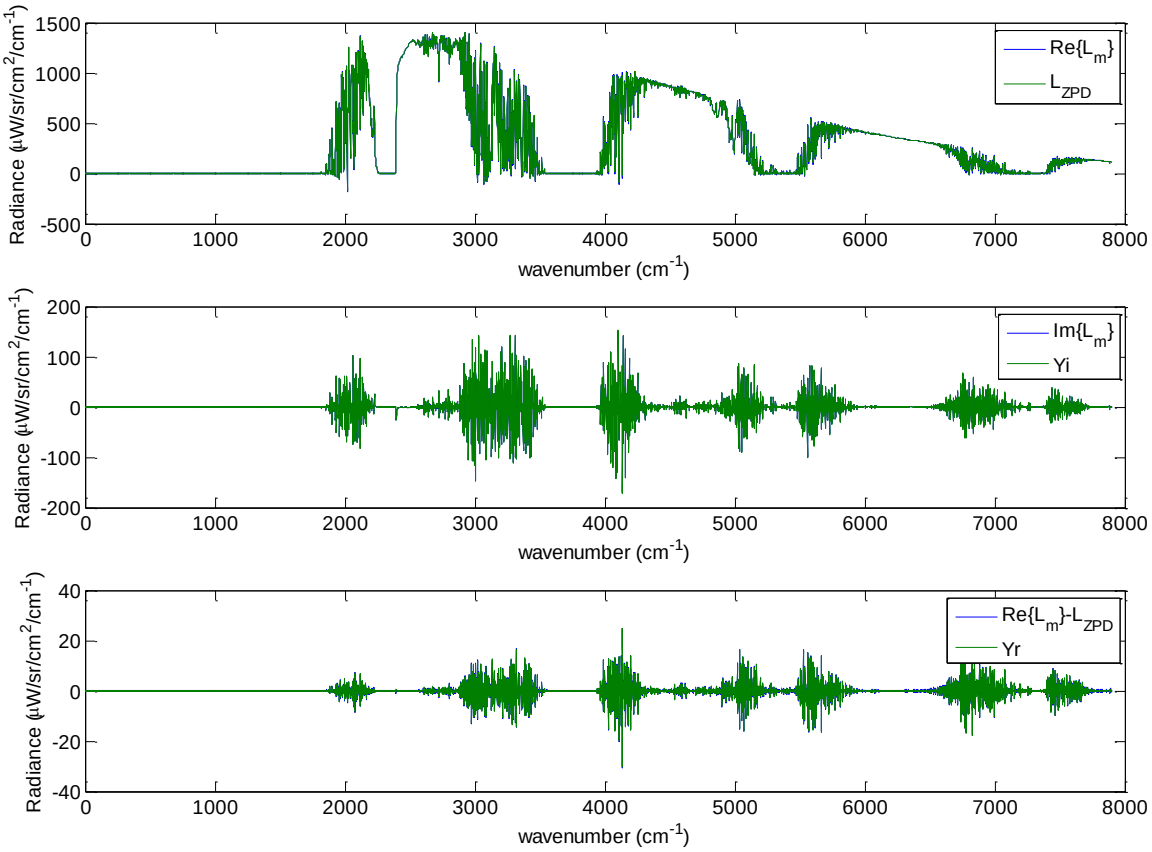

Figure 4. FTS spectrum of black body with atmospheric transmission path length of .5 km and a temperature change from 1500 K to 1200 K during data acquisition. MOPD = .25cm.

The corruption $\mathrm{Re}\{L_m\} - L_{ZPD}$ is a maximum of $20\mu W / sr / cm^2 / cm^{-1}$ whereas $\mathrm{Re}\{L_m\}$ has a maximum near $1400\mu W / sr / cm^2 / cm^{-1}$ meaning the corruption is a small fraction of the total signal. The matching of SCAs to wavenumber regions in the spectrum near highly varying spectral features confirms the derivative relationship to the magnitude of SCAs found in Equation (21). Large values of the derivative of the spectrum match with increased magnitude in SCAs.

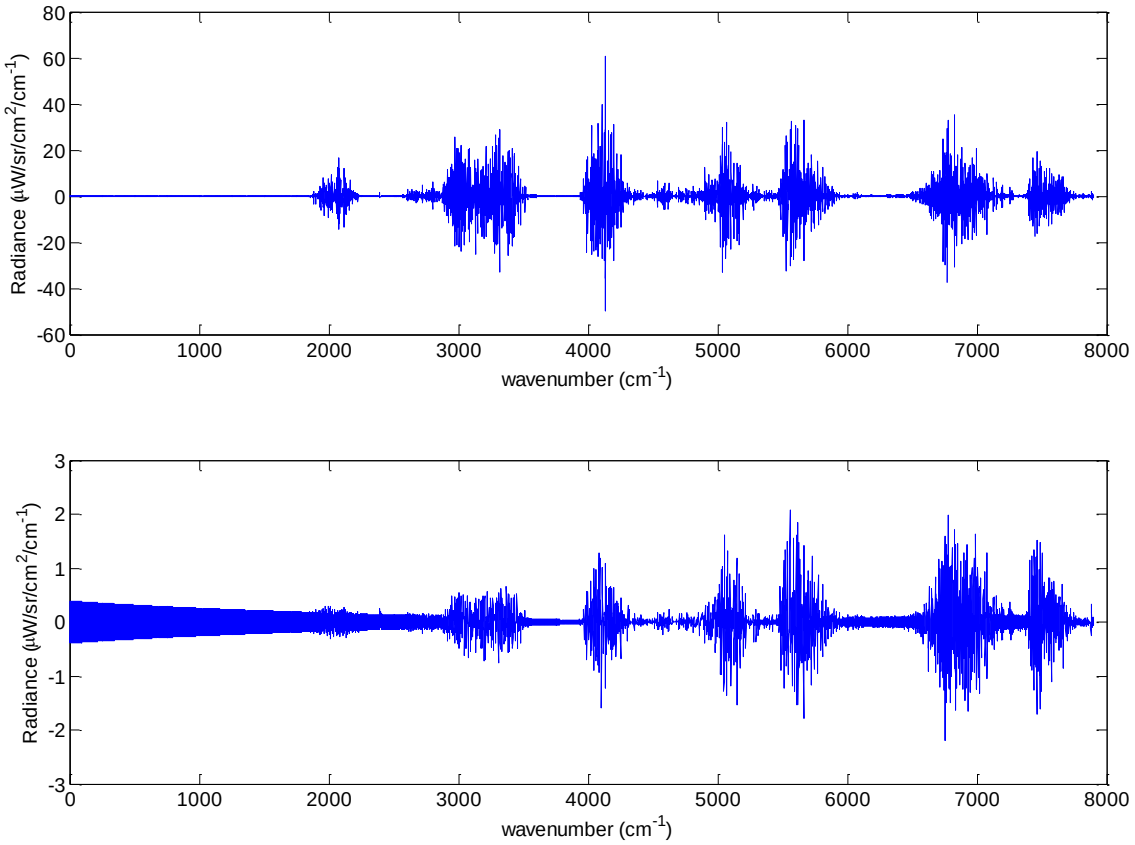

Figure 5. Top) Difference between Yi and $\mathrm{Im}\{L_m\}$ for Figure 4. Bottom) Difference between $\mathrm{Re}\{L_m\} - L_{ZPD}$ and the Yr for Figure 4.

Figure 5 shows the deviation of the calculated spectrum from the theoretical spectrum for Figure 4 and ultimately how accurately Equation (21) can represent the scene change effects. There is a numerical noise floor that the features must rise above seen in 0 to 2000 cm^{-1} on the bottom graph. For the temperature change from 1500 K to 1200 K the mathematical expressions accurately approximate SCAs to within a 1 to 3 $\mu W / sr / cm^2 / cm^{-1}$ in the real spectrum and 10 to $30 \mu W / sr / cm^2 / cm^{-1}$ in the imaginary spectrum.

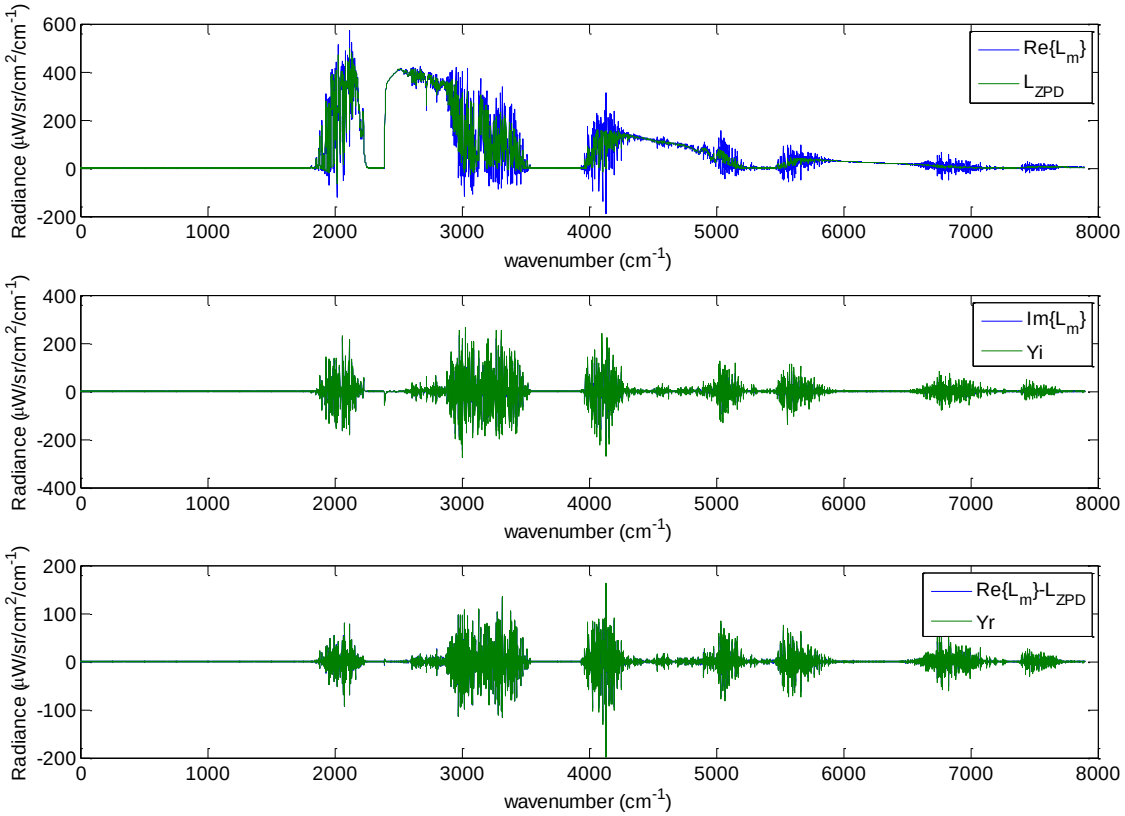

Figure 6. FTS spectrum of black body with atmospheric transmission path length of .5 km and a temperature change from 1500 K to 600 K during data acquisition. MOPD = .25cm

For the temperature change 1500 K to 600 K found in Figure 6, the same analysis is no longer accurate in mathematically describing the spectral change over time. $\mathrm{Re}\{L_m\} - L_{ZPD}$ now has a maximum value near $100 \mu W / sr / cm^2 / cm^{-1}$ which is of equal magnitude to the maximum values of $\mathrm{Re}\{L_m\}$ at $450 \mu W / sr / cm^2 / cm^{-1}$ meaning the corruption represents a larger fraction of the total spectral radiance. This is also seen the difference between maximum corruption magnitudes of approximately

$100\mu W / sr / cm^2 / cm^{-1}$ for Figure 6 and approximately $20\mu W / sr / cm^2 / cm^{-1}$ for Figure 4.

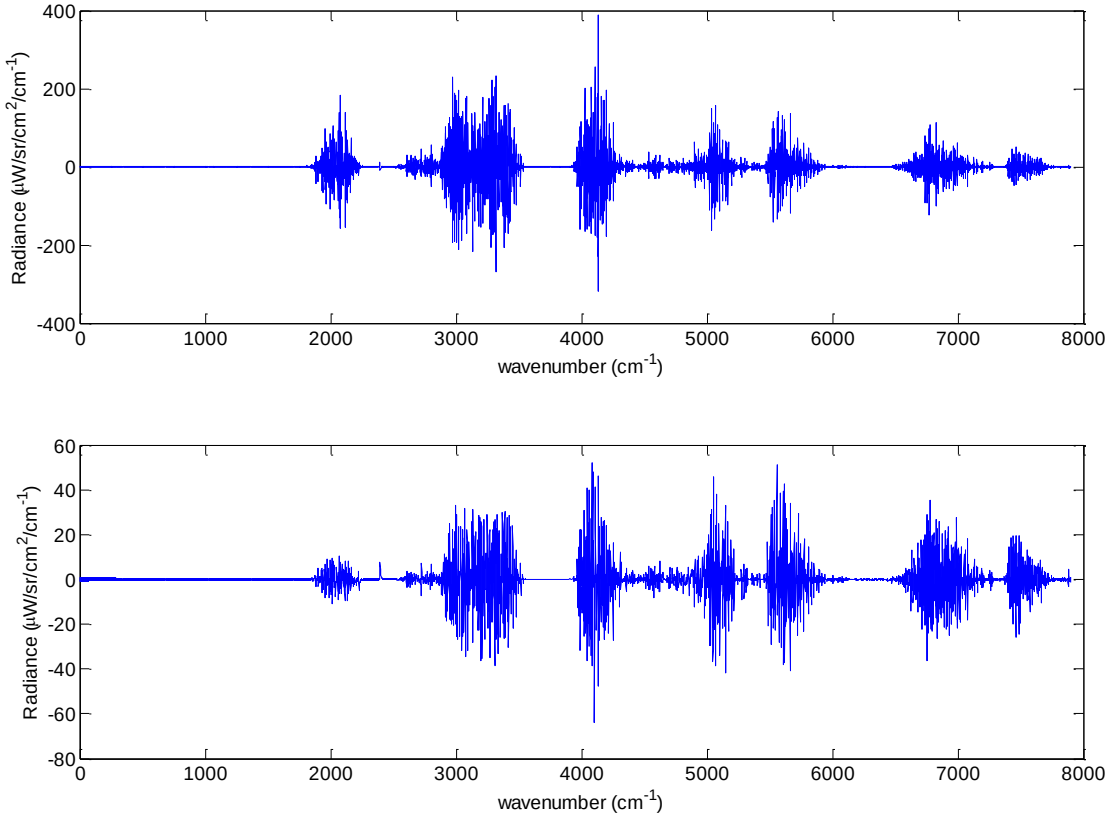

Figure 7. Top) Difference between Yi and $\mathrm{Im}\{L_m\}$ for Figure 6. Bottom) Difference between $\mathrm{Re}\{L_m\} - L_{ZPD}$ and the Yr for Figure 6.

There is significant difference between $\mathrm{Re}\{L_m\} - L_{ZPD}$ that cannot completely be accounted for by Yr. Similarly, $\mathrm{Im}\{L_m\}$ begins to deviate from the theoretical first order prediction, Yi. Higher order terms must be applied to account for $\mathrm{Re}\{L_m\} - L_{ZPD}$ and the difference between $\mathrm{Im}\{L_m\}$ and Yi. For the temperature change from 1500 K to 600 K,

the mathematical expression accurately approximate SCAs in Figure 7 with a maximum difference of $40\mu W/sr/cm^2/cm^{-1}$ in the real spectrum and $200\mu W/sr/cm^2/cm^{-1}$ in the imaginary spectrum. The magnitudes of the features are greater than that of Figure 5 due to the greater temperature change.

To show how much deviation between $\mathrm{Re}\{L_m\}$ and L_{ZPD} exists for the total spectrum and how it relates to $\mathrm{Im}\{L_m\}$, Figure 8 compares the change in the RMS of $\mathrm{Im}\{L_m\}$ with the RMS value of $\mathrm{Re}\{L_m\}-L_{ZPD}$ both as a function of the exponential decay constant, k, multiplied by the measurement time, t_{tot}. All values are normalized by the RMS of $\mathrm{Re}\{L_m\}$. Some differences between MOPD models could be created from defining the number of points in Equation (31) which depends on the MOPD and ultimately affects the spectral resolution of the input spectrum.

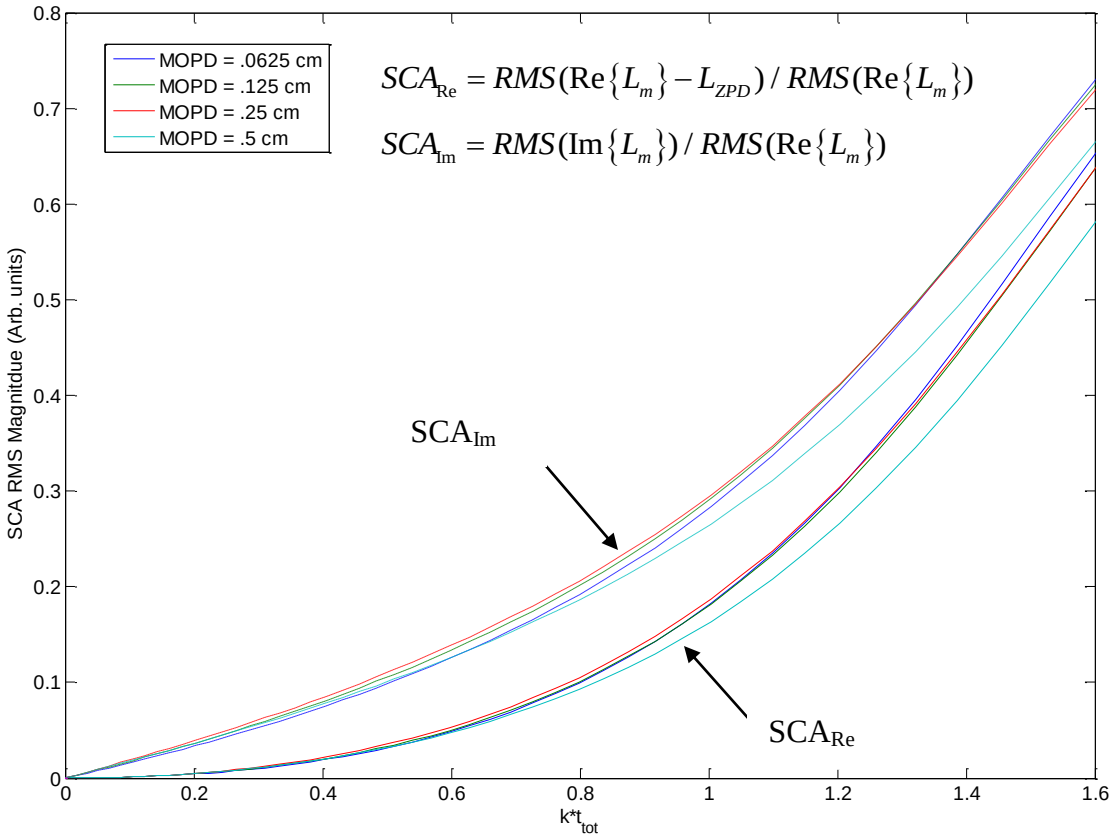

Figure 8. SCA_{Re} (solid) and SCA_{Im} (dashed) relationship with $k*t_{tot}$. Atmospheric transmission path length = .5 km.

To better allow for comparisons, the x-axis in Figure 9 was transformed into a percent change in temperature to better show how the RMS of $\mathrm{Im}\{L_m\}$ and the RMS of $\mathrm{Re}\{L_m\} - L_{ZPD}$ changed. This also allows for further comparison between different spectra. For these spectra, temperature changes of 55% yield a SCA_{Re} value of under 10%, meaning that for temperature changes of up to 55% the RMS of the corruption remains under 10% of the RMS spectrum value. If $\mathrm{Re}\{L_m\}$ matched L_{ZPD}, then the RMS value of the difference would be zero. In general, $\mathrm{Im}\{L_m\} > \mathrm{Re}\{L_m\} - L_{ZPD}$ for all

temperature changes and $\mathrm{Im}\{L_m\}$ grew faster than $\mathrm{Re}\{L_m\} - L_{ZPD}$ with temperature change.

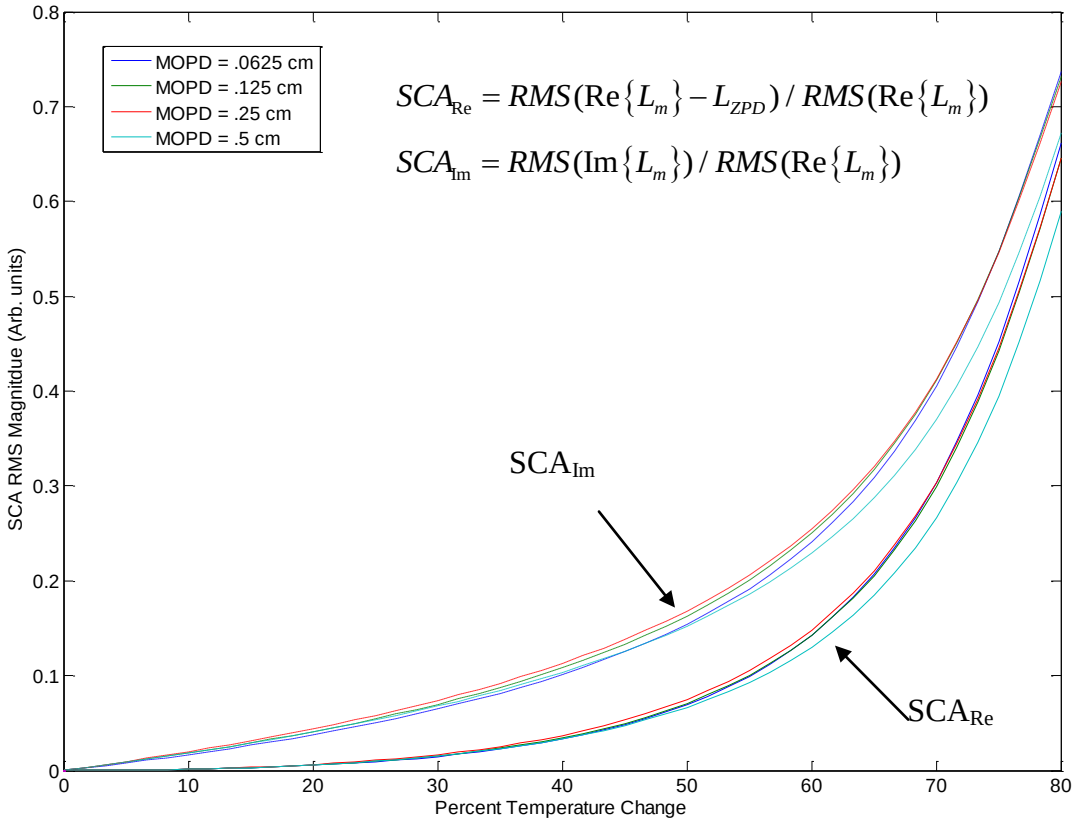

Figure 9. SCA_{Re} (solid) and SCA_{Im} (dashed) relationship with temperature change. Atmospheric transmission path length = .5 km.

Instead of comparing RMS values, the maximum values were explored in Figure 10. Sharp peaks in the imaginary spectrum come from large values in the derivative of the spectrum which are often the result of spectral absorption features. How well the theoretical predictions match the spectrum at those points is very important to accurately interpret the forensics of an explosion. Certain spectral features can often be several times the RMS value of the spectrum.

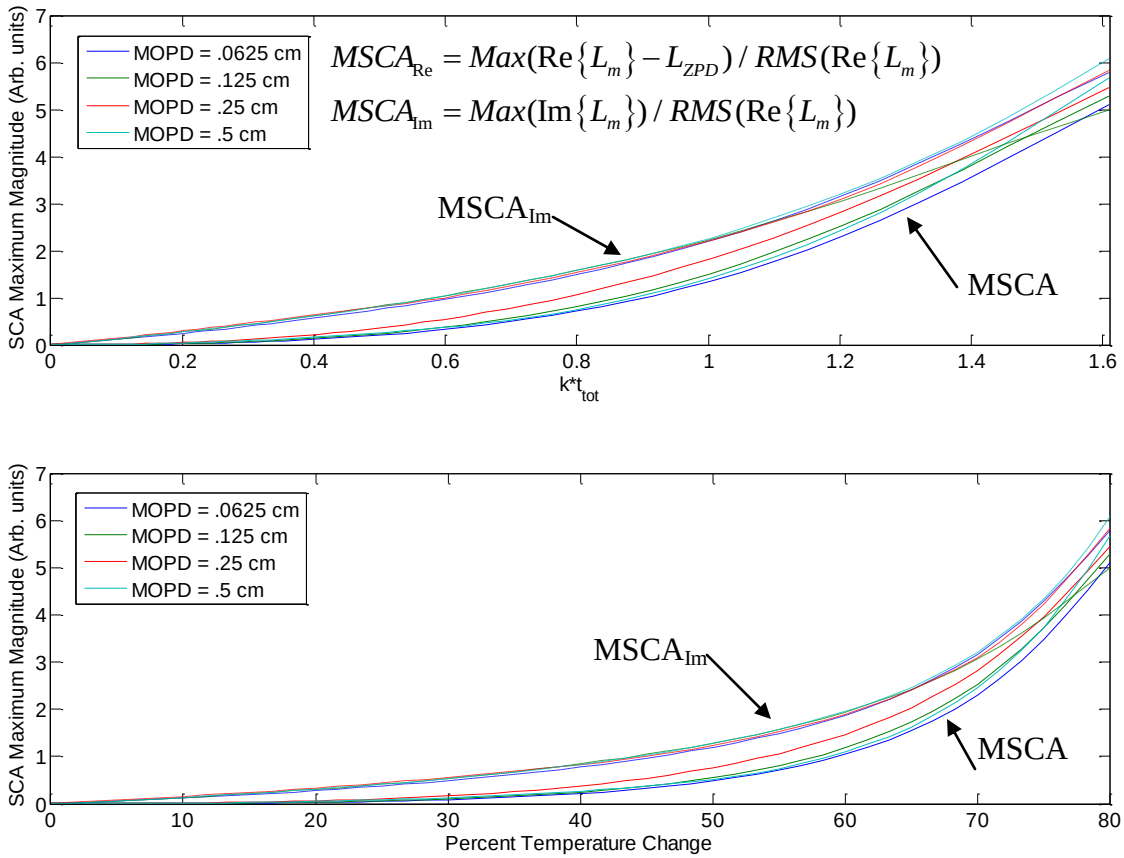

Figure 10. $MSCA_{Re}$ (solid) and $MSCA_{Im}$ (dashed) relationship with $k*t_{tot}$ on the top graph and with temperature change on the bottom graph. Atmospheric transmission path length = .5 km.

While this analysis is spectrum dependent, Figure 11 and Figure 12 show that by changing the temperature range and changing the atmospheric transmission features as a function of path length does not significantly change the deviation from L_{ZPD}.

Figure 11 provides three different maximum temperatures for starting decay parameters. For the three cases of starting temperatures 4000 K, 2500 K, and 1500 K decreasing to 20% of the original value, the general trend is the same showing that at

percent temperature changes under 50%, the RMS of $\mathrm{Re}\{L_m\} - L_{ZPD}$ remains under 10% of the RMS value of $\mathrm{Re}\{L_m\}$. The SCA RMS magnitudes of the different temperatures are in part due to their black body's overlap with the wavenumber region of interest 0 to 7901cm^{-1} and how much of the black body's power is contained within that region.

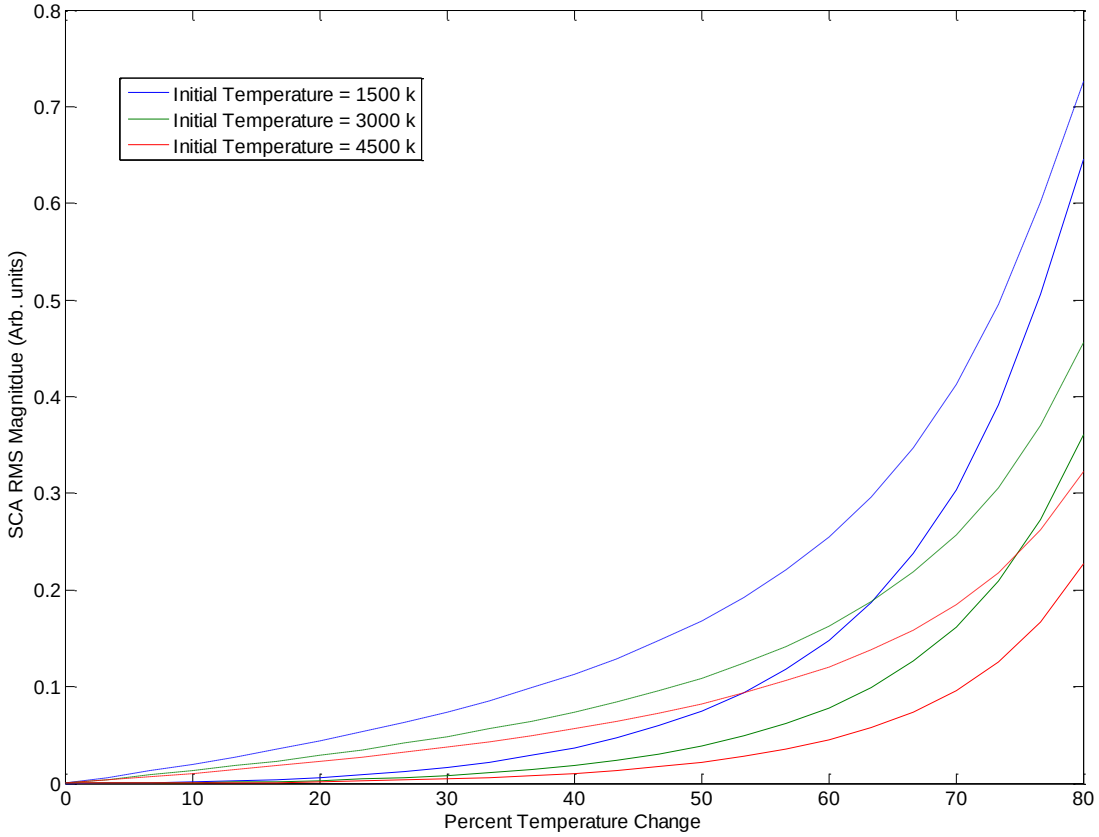

Figure 11. The three scenarios correspond to different initial temperatures of 1500 k, 3000 k, and 4500 K. Dashed lines represent the SCA_{Im} while the solid lines represent the SCA_{Re}. MOPD = .5 cm and Atmospheric transmission path length = .5 km.

Figure 12 shows the same general conditions of initial temperature of 1500 K and an MOPD equaling .5 cm, only this time with different atmospheric path lengths of .5 km, 1 km and 2 km. This results in the transmission function τ_{atm} having different magnitudes on certain spectral features. For all the cases, the general trend holds and for percent temperature changes under 55%, the RMS of $\mathrm{Re}\{L_m\} - L_{ZPD}$ remains under 10% of the RMS value of $\mathrm{Re}\{L_m\}$ and $\mathrm{Im}\{L_m\} > \mathrm{Re}\{L_m\} - L_{ZPD}$.

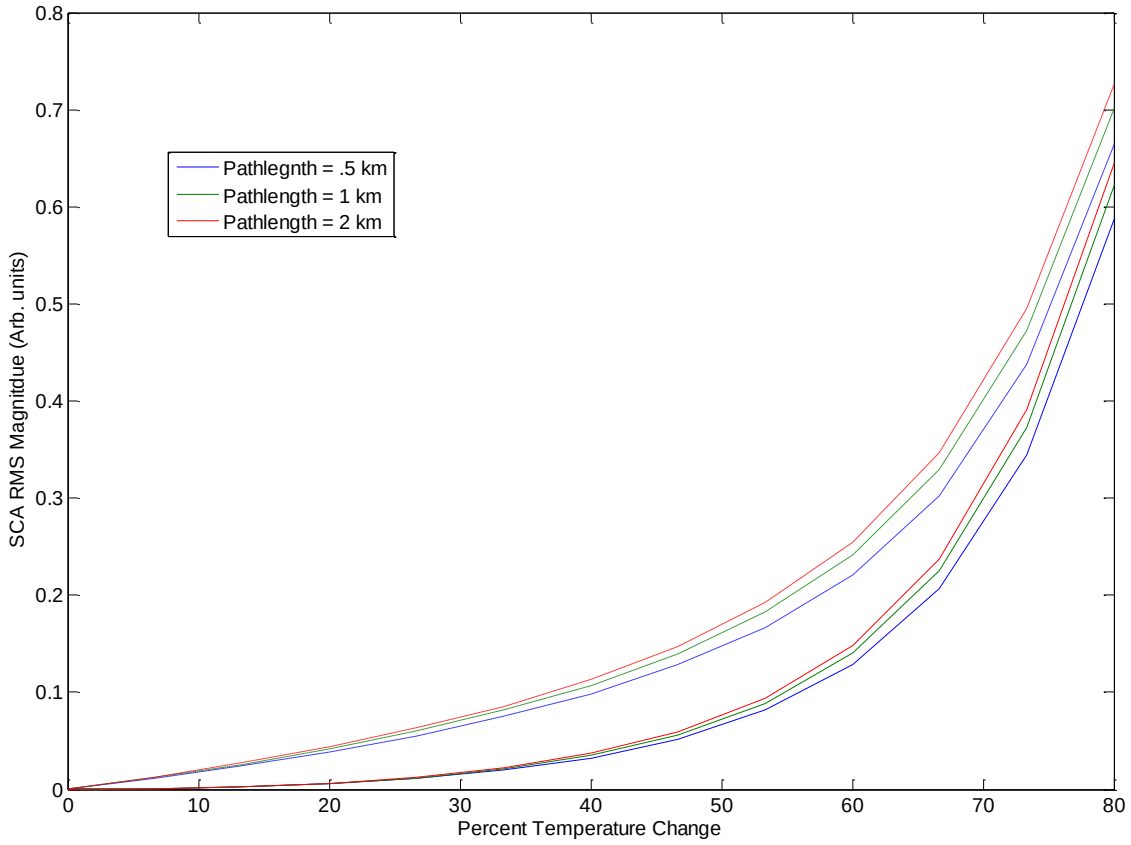

Figure 12. The three scenarios correspond to different atmospheric transmission profiles as a function of the path lengths of .5 km, 1 km, and 2 km. Dashed lines represent the SCA_{Im} while the solid lines represent the SCA_{Re}. MOPD = .5 cm.

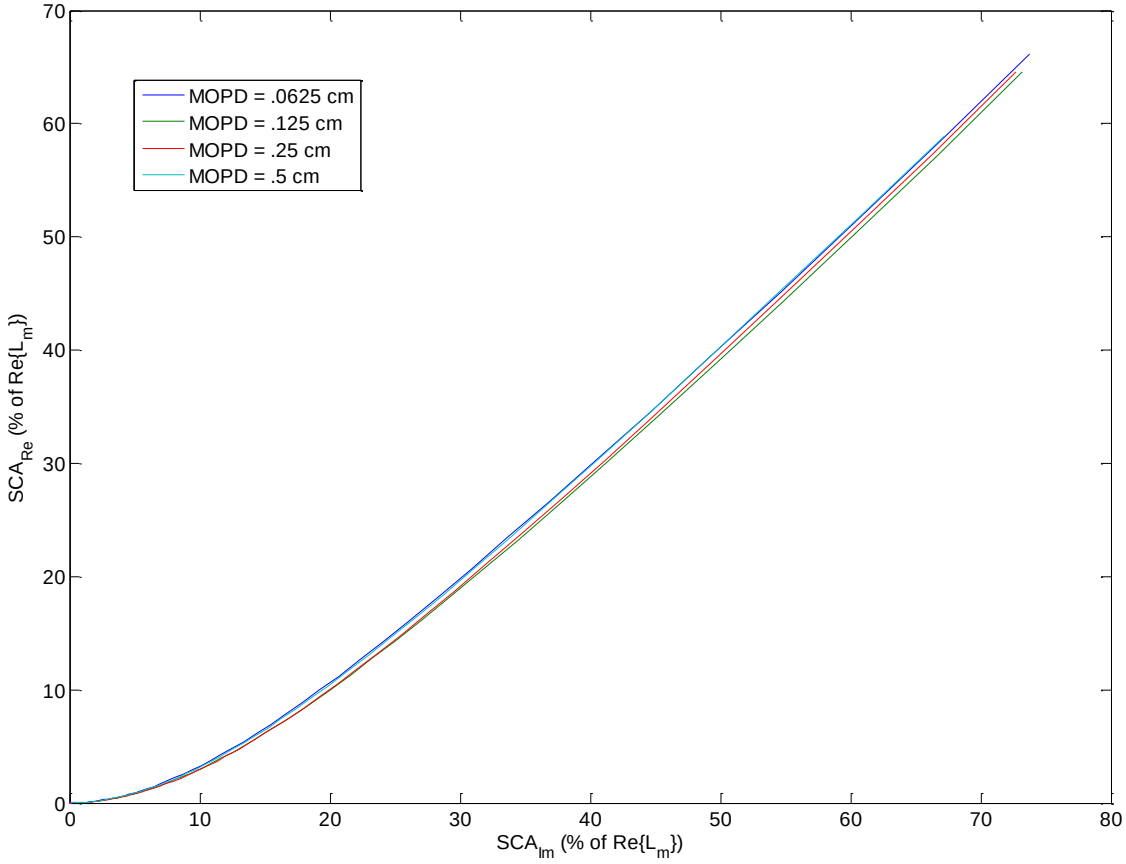

Figure 13. Relationship between SCA_{Im} and SCA_{Re}. Axes are shown as a percent of the RMS of $\mathrm{Re}\{L_m\}$.

To be able to use the imaginary spectrum to help predict discrepancies between $\mathrm{Re}\{L_m\}$ and L_{ZPD}, Figure 13 shows their relationship. After the RMS of $\mathrm{Im}\{L_m\}$ reaches 15% of the RMS of $\mathrm{Re}\{L_m\}$, the RMS of $\mathrm{Re}\{L_m\} - L_{ZPD}$ has a linear relationship with the RMS of $\mathrm{Im}\{L_m\}$. It appears that SCA_{Im} is about 10% higher than SCA_{Re}, meaning a spectrum with $SCA_{Im} = 40\%$ of $\mathrm{Re}\{L_m\}$ has a $SCA_{Re} = 30\%$ of $\mathrm{Re}\{L_m\}$.

The usefulness of Equation (21) as an approximation for a exponentially cooling Planckian radiance viewed by a FTS can be seen in Figure 14 that show the deviation of the calculated values in the model from the theoretical values.

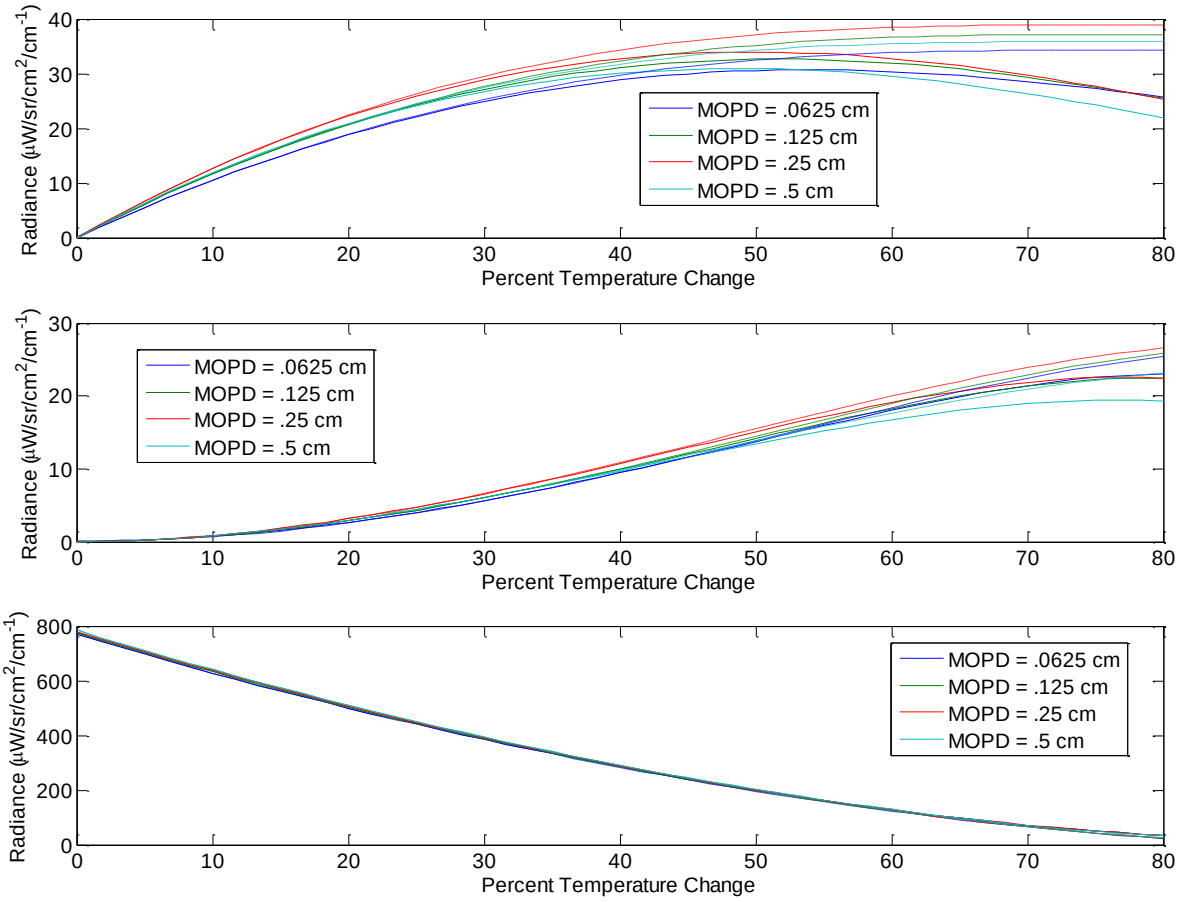

Figure 14. Dashed lines represent theoretical predictions based on implementing Equation (21) based on Kick et al. The solid line represents the actual modeled values. Top) Deviation of RMS values of $\mathrm{Im}\{L_m\}$ and Yi. Middle) Deviation of the RMS of $\mathrm{Re}\{L_m\} - L_{ZPD}$ and Yr. Bottom) Deviation of the RMS of $\mathrm{Re}\{L_m\}$ from the RMS of L_{ZPD}.

The deviation from theoretical predictions is clearly seen in the graphs on Figure 14. For temperature changes up to 40%, the values of Equation (21) provide an accurate approximation. For the bottom graph representing the difference between the RMS of L_{ZPD} and the RMS of $\mathrm{Re}\{L_m\}$, all lines lie on top of one another indicating that the average values do no significantly diverge from theoretical calculations for RMS values.

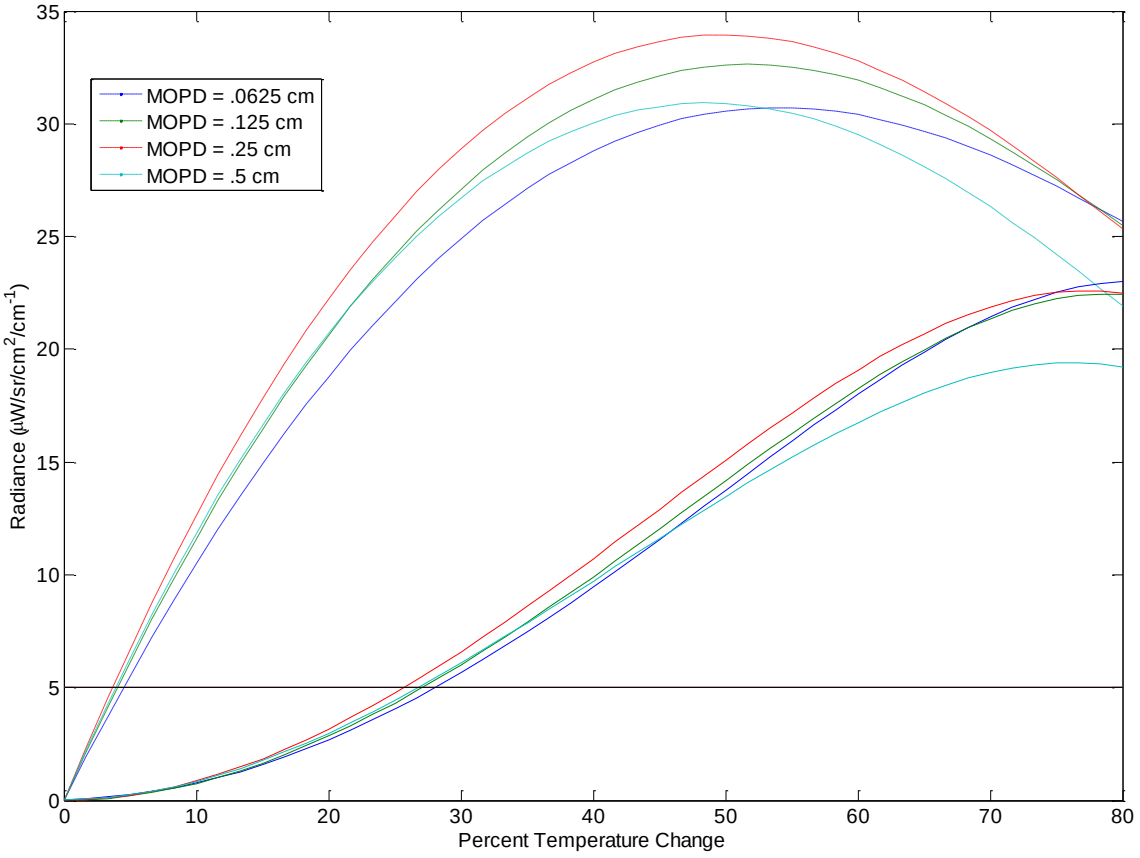

Figure 15. RMS of $\mathrm{Im}\{L_m\}$ (dashed) and the RMS of $\mathrm{Re}\{L_m\} - L_{ZPD}$ (solid) values as they change with temperature change. The black horizontal line represents a NESR of $5\mu W / sr / cm^2 / cm^{-1}$ that both $\mathrm{Im}\{L_m\}$ and $\mathrm{Re}\{L_m\} - L_{ZPD}$ must rise above for SCAs to be distinguishable.

Figure 15 shows the evolution of RMS SCA magnitudes with temperature change and provides a comparison to a NESR that a SCA magnitude must surpass to rise above the noise floor. While the RMS values may be under or over the NESR individual SCA magnitudes at a specific wavenumber may or may not be above the NESR indicating a need for analysis of individual wavenumber SCAs.

IV. Experiment

Experimental setup

To experimentally characterize spectral artifacts due to a changing source, a variable input lamp was observed by an FTIR. The ABB-Bomem MR154, a dual channel interferometer with an internal cold reference, was used to collect spectra in the mid infrared. The instrument was configured with InSb (1.6-5.6μm) and HgCdTe (2.0μm - 20μm) detectors. All scans with the FTIR were done at a resolution of 1 cm^{-1} to slow down the acquisition rate resulting in running a collection frequency of 1.17 Hz. An Oriel Q series incandescent lamp was used as the variable light source despite the limited overlap in the infrared region of the detectors. The lamp envelope and optics have a passband of approximately 0.2μm to 2.5μm. Convolving the passband of the lamp envelope, the Germanium blocking filter and the InSb detector response yields an approximate range of 1.8μm-2.8 μm for the response due to the lamp filament. Only the InSb channel was able to capture the signal as the HgCdTe was outside the passband.

The setup in Figure 16 shows the relationship between the lamp and the FTIR. All incident light goes through the Germanium window to control the wavelengths involved in the interferogram and to stop aliasing from higher wavelengths. Possible scattered light can reach the detectors from dust on the optics although this is assumed to be negligible.

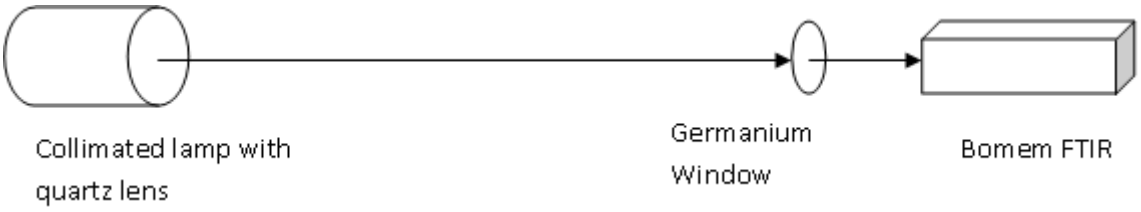

Figure 16. Experimental Setup

For reference, 30 interferograms were taken for static lamp powers descending from 210 W in 7 Watt increments. A total of ten measurements were made for each point. Each measurement made was a 1/2 scan resulting in each power level being scanned in two different directions. Each scan direction might not have the same properties so they must be accounted for separately. This gave five measurements in each scan direction that was averaged together to increase signal to noise.

Changing source interferograms were taken during power decay over the same Watt range as above; however, interferograms were taken while the source was changing. Two trials were performed, the first with a total of 50 measurements, 25 in each direction, and the second with 75 measurements, 38 in direction one and 37 in direction two. The FTIR started taking measurements and the lamp was then triggered after some time to decrease from 210 W to zero. The interferograms were the converted into spectra and phase corrected using code provided by Bomem.

Experiment analysis

Viewing the changing lamp provided insight into the detection of SCAs. The imaginary part created from SCAs must be deconvolved from the regular noise associated with an imperfect system. The noise floor of the instrument was too high for the percent

change capable of the lamp combined with the signal magnitude to be able to distinguish significant SCAs in the imaginary spectrum. Using the same analysis found in the model is difficult when the overall structure of the imaginary spectrum is hidden within the instrument noise, however, over certain regions in the spectrum with sharp changes, imaginary peaks above the noise level could be detected.

Figure 17 provides the time evolution of the interferogram ZPD voltage for each scene change interferogram. Each point represents a different interferogram ZPD voltage. Assuming no dwell time between scans and using a scan rate of 1.17 Hz, the starting voltage level for the scene change interferogram ZPD was assumed to be the voltage level linearly interpolated to 3/7 seconds before the ZPD voltage.

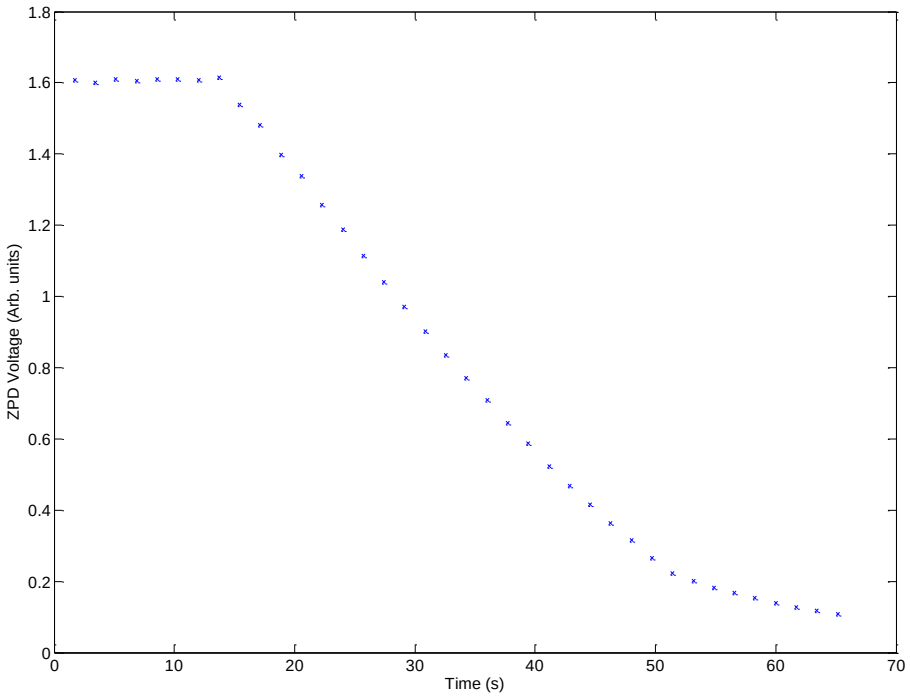

Figure 17. SCA interferogram ZPD voltage evolving with time.

Similarly, the ending scene change interferogram ZPD voltage was determined by linearly interpolating 3/7 seconds after the scene change interferogram ZPD voltage on Figure 17.

Figure 18 shows the spectrum of Measurement 10 at 17.14 seconds which corresponds to the beginning of the decline in input power. The spectral features from approximately 2500 cm^{-1} to 5500 cm^{-1} can be seen to represent the spectral features caused by the filament in the lamp but they were unable to change fast enough to produce sizeable SCA magnitudes. The imaginary components rising above the noise level near 3900 cm^{-1}, 4900 cm^{-1}, and 5250 cm^{-1} are noticeable in the spectra taken close to the initial starting point of the radiance decline. The 3900 cm^{-1} and 5250 cm^{-1} peaks could be attributed to the change in radiance over the acquisition time being able to create imaginary spectral features that could rise above the noise floor however the 4900 cm^{-1} peak does not coincide with a highly structured spectrum so its cause is unknown. The spectral features found around 2000 cm^{-1} served as a reference for every spectrum because they did not significantly change during the entire data acquisition.

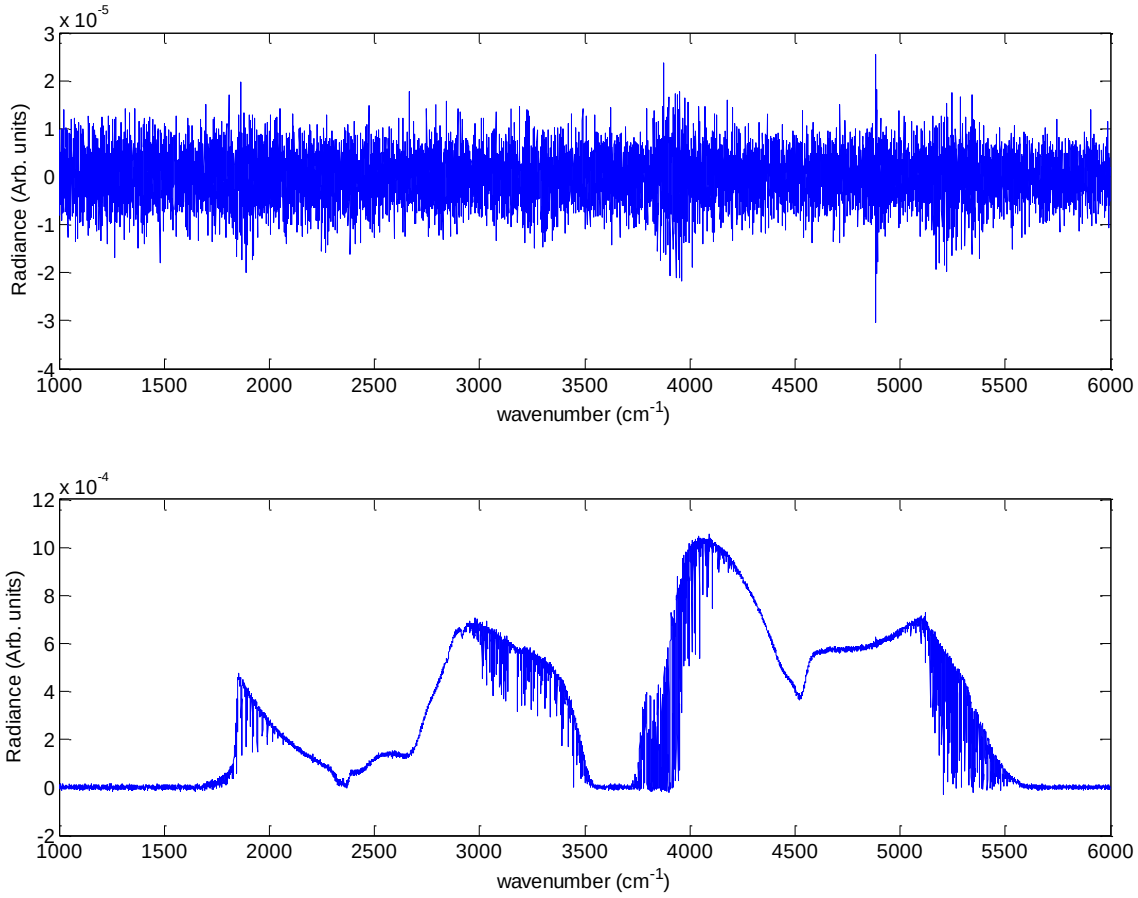

Figure 18. Measurement 10 spectrum at 17.14 seconds with a ZPD voltage = 1.481 V, imaginary on top and real on bottom, of a decaying incandescent lamp. Measurement time corresponds to a few SCA spectral peaks in the imaginary spectrum.

As the lamp radiance begin to decline, spectral features were no longer easily observable because the overall signal magnitude was too small. Figure 19 shows the spectrum of Measurement 25 which corresponds to near the middle of the 210 W to 0 W range at 42.86 seconds. The radiance magnitude was unable to provide significant and easily recognizable imaginary spectral features as seen before.

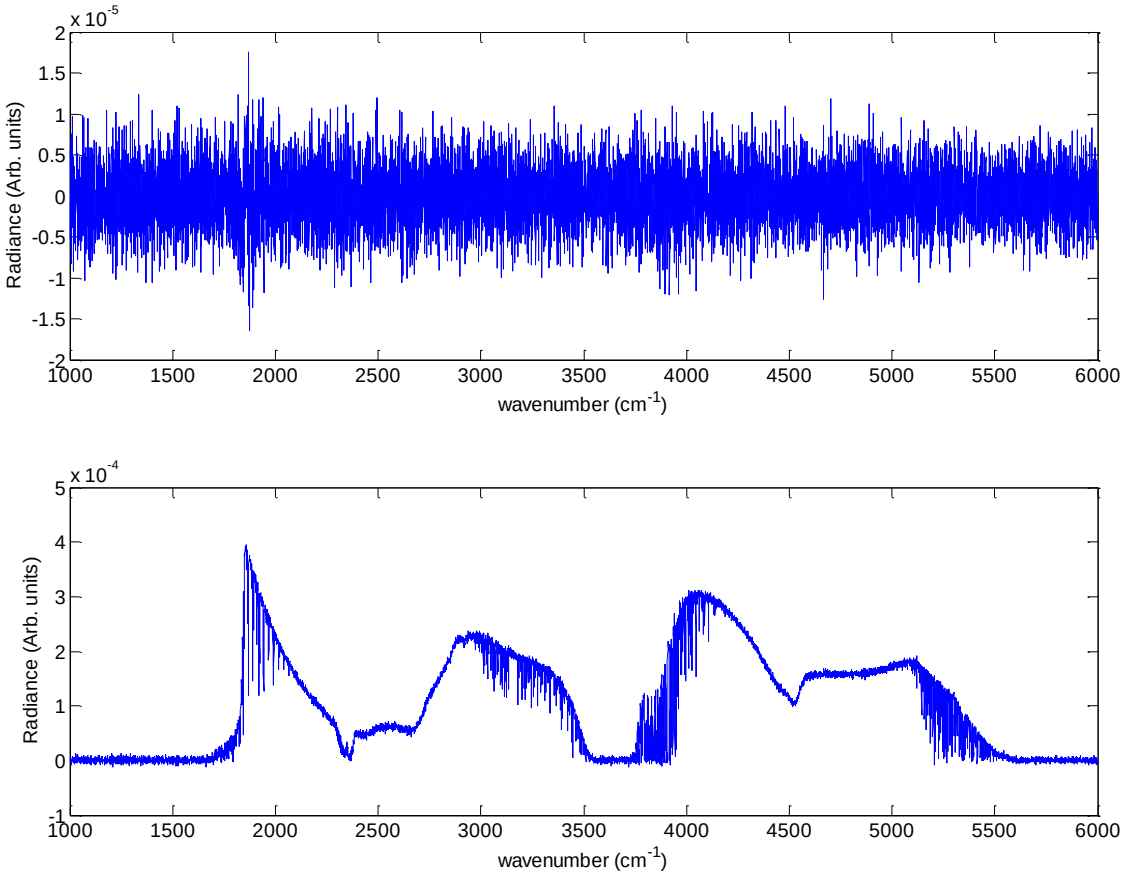

Figure 19. Measurement 25 spectrum at 42.86 seconds with a ZPD voltage = 0.47 V, imaginary on top and real on bottom, of a decaying incandescent lamp. Measurement time corresponds to a radiance magnitude and change that created no noticeable SCA imaginary spectral features.

To compare the magnitude of the few SCA spectral lines in the scene change spectrum to the change in ZPD voltage that occurred during the scan, the difference in ZPD voltage was calculated using interpolated values based on Figure 17. To quantify the magnitude of SCAs, an RMS NESR was calculated for wavenumbers next to the SCA

location where there was only noise. The RMS NESR was calculated by selecting an interval near the region of interest and extracting the largest positive and negative peaks to determine a peak to peak NESR. The RMS NESR is then

$$RMSNESR = \frac{NESR_{PtP}}{6}.^{[9]} \tag{36}$$

For Figure 18, the few imaginary peaks above the noise floor near 3900 cm^{-1} reached a value of 54.8% above the RMS NESR for ZPD voltage changes of 2.52%. Since $\mathrm{Im}\{L_m\} > \mathrm{Re}\{L_m\} - L_{ZPD}$, it is not unreasonable to assume that any corruption in the real spectrum is small and the accuracy in the spectrum is only limited by the noise level of the instrument. While the ZPD voltage change was higher for Measurement 25 at 7.14%, the signal magnitude was smaller than the noise so no peaks emerged above NESR.

V. Conclusions

Interpretation of scene change effects in observing detonation fireballs

The nature of scene change on FTS provides an extra layer of complexity in interpreting spectra from transient events. Using an approximation given by Equation (21) can mathematically describe this complexity when the temperature change creates a change in the scene radiance described by Kick et al.

Regardless of mathematical representation, quantifying the structure and magnitude of SCAs and analyzing $\mathrm{Im}\{L_m\}$ acquired by a FTS as a percentage of $\mathrm{Re}\{L_m\}$ provides insight into the approximation of $\mathrm{Re}\{L_m\}$ as L_{ZPD} and the resulting level of corruption. This is useful in understanding the accuracy of using FTS on detonation fireballs. When τ_{atm} is highly structured, the magnitude of SCAs increases because of the increased derivative found where spectral features are present. The ratio of SCA magnitude to the total spectrum also increases as temperature changes and in general, $\mathrm{Im}\{L_m\} > \mathrm{Re}\{L_m\} - L_{ZPD}$. These trends were independent of initial temperature, spectral resolution, or τ_{atm}. For a MOPD = 0.5cm, a drop in temperature of 3.3% during data acquisition created a RMS value of $4.3\mu W / sr / cm^2 / cm^{-1}$ and interpolating to a temperature change of 3.95% gave the desired $5\mu W / sr / cm^2 / cm^{-1}$. For the same conditions, a temperature decline of 26.7% gave the same RMS radiance value of $5\mu W / sr / cm^2 / cm^{-1}$.

Observing a lamp with declining input power provided only a few spectral features in the imaginary spectrum that were larger than the noise floor associated with

the instrument. If SCAs are below the NESR for the detection instrument then the accuracy of the spectrum is only limited by the NESR of the instrument. The few spectral features were 54.8% above RMS NESR for a ZPD voltage change of 2.52% during data acquisition that lasted 6/7 seconds. Since the imaginary SCAs were hardly noticeable, it is not unreasonable to assume $\mathrm{Re}\{L_m\} - L_{ZPD}$ is negligible.

Recommendations

Future work could analyze specific spectral features to show the corruption on spectral features of interest rather than a RMS value for the whole spectrum. This would be especially important when focusing on CO_2 and H_2O bands commonly found in detonation fireball spectra. The addition of higher order terms in the analysis would also more accurately describe scene change effects on radiance mathematically. While there might be significant corruption to specific spectral features, the overall spectrum can still be fit to a Planckian for blackbody temperature determination.

References

[1] Gross, Kevin. "Phenomenological model for infrared emissions from high explosive detonation fireballs," Air Force Institute of Technology, Ph. D. dissertation AFIT/DS/ENP/07-03, 2007.

[2] J.W. Brault, “Fourier transform spectrometry,” in High Resolution in Astronomy, A. Benz, A. Huber, and M. Mayor, eds. (Geneva Observatory, Sauverny, Switzerland, 1985), pp. 1-61.

[3] L. Sromovsky, “Radiometric errors in complex Fourier transform spectroscopy”, Applied Optics Vol. 42 No. 10 (2003)

[4] R. J. Bell, Introductory Fourier Transform Spectroscopy. Academic Press Inc, c 1972

[5] W. H. Press, S. A. Teukolsky, W. T. Vetterling, and B. P. Flannery, Numerical Recipes (Cambridge U. Press, Cambridge, UK, 1992).

[6] H. Kick, V. Tank and E. Lindermeir, “Impact of scene changes during data acquisition in Fourier spectroscopy,” Journal of Quantitative Spectroscopy & Radiative Transfer 92 (2005) pg. 447-455.

[7] Marko H. Methoden der Systemtheorie. 2nd ed. Berlin: Springer. p. 90.

[8] Discussion with Dr. Kevin Gross about the finite nature of a realistic Michelson versus the ideal full transform found in Kick et al.

[9] ‘NESR Measurements”. Bomem MR Series Alignment Proceducres, Chapter 8, pg 27.

REPORT DOCUMENTATION PAGE	Form Approved OMB No. 074-0188

1. REPORT DATE *(DD-MM-YYYY)*	2. REPORT TYPE	3. DATES COVERED *(From – To)*
25-03-2010	Master's Thesis	August 2009 – March 2010

4. TITLE AND SUBTITLE

SCENE CHANGE ARTIFACTS IN FOURIER TRANSFORM SPECTROSCOPY OF TEMPORALLY CHANGING SOURCES

5a. CONTRACT NUMBER

5b. GRANT NUMBER

5c. PROGRAM ELEMENT NUMBER

6. AUTHOR(S)

Young, Anthony M., Second Lieutenant, USAF

5d. PROJECT NUMBER

5e. TASK NUMBER

5f. WORK UNIT NUMBER

7. PERFORMING ORGANIZATION NAMES(S) AND ADDRESS(S)
Air Force Institute of Technology
Graduate School of Engineering and Management (AFIT/EN)
2950 Hobson Way, Building 640
WPAFB OH 45433-8865

8. PERFORMING ORGANIZATION REPORT NUMBER

AFIT/GAP/ENP/10-M16

9. SPONSORING/MONITORING AGENCY NAME(S) AND ADDRESS(ES)
National Air and Space Intelligence Center/ DAIR
4180 Watson Way
Wright Patterson AFB, OH 45433

10. SPONSOR/MONITOR'S ACRONYM(S)
NASIC

11. SPONSOR/MONITOR'S REPORT NUMBER(S)

12. DISTRIBUTION/AVAILABILITY STATEMENT

APPROVED FOR PUBLIC RELEASE; DISTRIBUTION UNLIMITED.

13. SUPPLEMENTARY NOTES

14. ABSTRACT

Improved understanding of midwave infrared (1-5 micron) spectral emissions from detonation fireballs is needed to develop phenomenological models for battle space optical forensics. The ability to measure radiance over a wide band pass at arbitrary resolutions make Fourier-transform spectrometers (FTS) an attractive tool. However, interferometer based spectroscopic measurements can be corrupted when the observed intensity changes during data acquisition. While small, random fluctuations in scene intensity translate into noise, systematic variations introduce scene-change artifacts (SCAs) into Fourier-transformed spectrum. Approximating a detonation fireball as a blackbody radiator, modified with an atmospheric attenuation τ_{atm}, with an exponentially cooling temperature $T(t) = T_0 e^{-kt}$, double sided interferograms from an ideal Michelson interferometer were simulated and converted to a measured spectrum L_m to characterize the nature and magnitude of SCAs. With $T_0 = 1500K$, changing scene spectra on $0 < \tilde{\nu} < 7900cm^{-1}$ at $\delta\tilde{\nu} = 0.04cm^{-1}$ resolution were computed with percent changes in $T(t)$ between 0 and 80%. The real part of L_m ($\mathrm{Re}\{L_m\}$) is well approximated by the instantaneous spectrum (L_{ZPD}) at zero path difference. Differences between $\mathrm{Re}\{L_m\}$ and L_{ZPD} ($\mathrm{Re}\{L_m\} - L_{ZPD}$) is largest when τ_{atm} is highly structured and these differences increase with the amount of temperature change during the measurement. Similarly, the imaginary part of L_m ($\mathrm{Im}\{L_m\}$) exhibits highly structured features whenever τ_{atm} changes rapidly with V. In general, $\mathrm{Im}\{L_m\} > \mathrm{Re}\{L_m\} - L_{ZPD}$ agreeing with previous theoretical work and the increase in magnitude of $\mathrm{Im}\{L_m\}$ with temperature change is more pronounced than $\mathrm{Re}\{L_m\} - L_{ZPD}$. These trends were independent of initial temperature, spectral resolution, or choice of τ_{atm}. For a MOPD = .5cm, a 4% reduction in temperature during a single scan produced an RMS value of $5\mu W / sr / cm^2 / cm^{-1}$ in $\mathrm{Im}\{L_m\}$. A 27% temperature change was needed to produce the same RMS value for $\mathrm{Re}\{L_m\} - L_{ZPD}$. For comparison, the RMS value of L_{ZPD} was $507\mu W / sr / cm^2 / cm^{-1}$ and $125\mu W / sr / cm^2 / cm^{-1}$ for a 20% and 60% temperature change, respectively. SCAs were also studied with an ABB/Bomem MR-154 FTS by measuring a time-varying broadband source. Using an Oriel Q-series incandescent lamp, the FTS operating at $1cm^{-1}$ resolution observed the changing spectral radiance as the lamp's input power was smoothly varied during interferogram acquisition. A 2.52% relative change in ZPD voltage during the scan produced a few spectral lines in $\mathrm{Im}\{L_m\}$ that were 54.8% above the instrument RMS NESR.

15. SUBJECT TERMS
asymmetric interferograms, scene-change artifacts, Fourier transform spectroscopy

16. SECURITY CLASSIFICATION OF:			17. LIMITATION OF ABSTRACT	18. NUMBER OF PAGES	19a. NAME OF RESPONSIBLE PERSON
a. REPORT	b. ABSTRACT	c. THIS PAGE			Dr. Kevin Gross
U	U	U	UU	56	19b. TELEPHONE NUMBER *(Include area code)* (937) 255-6565, ext 4558 (kevin.gross@afit.edu)

Standard Form 298 (Rev. 8-98)
Prescribed by ANSI Std. Z39-18